J Mol Model (2011) 17:1051–1060
DOI 10.1007/s00894-010-0802-9

ORIGINAL PAPER

Study of ring influence and electronic response to proton transfer reactions. Reaction electronic flux analysis

Barbara Herrera

Received: 5 May 2010 / Accepted: 6 July 2010 / Published online: 25 July 2010

Abstract In this article, a theoretical study of 1–5 proton transfers is presented. Two model systems which represent 1–5 proton transfer, 3-hidroxy-2-propenimine and salicyldenaniline have been studied as shown in Fig. 1. For this purpose, a DFT/B3LYP/6-311+G**, reaction force and reaction electronic flux analysis is made. The obtained results indicate that both proton transfers exhibit energetic and electronic differences emphasizing the role of the neighbor ring and the impact of conjugation on electronic properties.

Keywords Proton transfer · Reaction electronic flux · Reaction force

Introduction

In biological systems hydrogen bonds are structural elements that in many cases stabilize the system and are responsible for specific reactivity patterns of both donor and acceptor atoms. Proton transfers (PT) are basic dynamic processes that occur in hydrogen-bonded molecules, they mostly take place between a donor (D) on a polar bond, usually CH, NH or OH, and a polar neighboring acceptor atom (A) bearing a negative charge.

Recently the application of new concepts of reactivity such as *reaction force* (F(ξ)) and *reaction electronic flux* (REF) on 1–4 Hydrogen transfer between the donor atom and a neighbor acceptor atom, both separated by 2 atoms, has given important insights in systems ranging from simple aliphatic [1] to heteroatomic rings [2], finding that specific structural rearrangements activate the proton transfer and electronic reordering. When dealing with 1–5 proton transfers, D and A atoms are more spaced and questions arise wether the transfer occurs by the same 1–4 mechanism or it is assisted by other effects.

We have chosen two model systems which represent 1–5 proton transfer, 3-hidroxy-2-propenimine (**R1**) and salicyldenaniline (**R2**) depicted in Fig. 1. It is well known by experimental and theoretical works that salicylic-acid related compounds present proton transfers which are assisted by an important electronic reorganization in neutral and ionized states [3–10].

In this paper, a density functional theory (DFT), DFT/B3LYP/6-311+G** study of the hydrogen-transfer reaction $D-H\cdots A \rightarrow D\cdots HA$, where D and A are oxygen and nitrogen atoms, is presented. The main goal of this work is to characterize the mechanism of 1,5 hydrogen transfer in **R1** and **R2** and stablish the nature of the ring influence on the electronic reordering that is taking place during the reactions.

Characterization of the mechanisms that activate the intramolecular hydrogen transfer can be achieved by monitoring different properties within the framework of the reaction force analysis; their critical points help confine the different mechanisms that might be operating within specific regions defined along the reaction coordinate. The reaction force profile, the negative derivative of the energy profile, and the simultaneous analysis of structural and electronic properties such as bond, angles, reaction electronic flux (REF) [11, 12], electronic populations and dipole moments, provide a complete picture of proton transfer reactions.

It has been proven in earlier works, that in an elementary step of the potential energy surface, characterized by a

This work was supported by FONDECYT under grants #11080002 and #1090460.

B. Herrera (✉)
QTC, Pontificia Universidad Católica de Chile,
Av. Vicuña Mackenna,
4860 Macul, Santiago, Chile
e-mail: bherrera@uc.cl

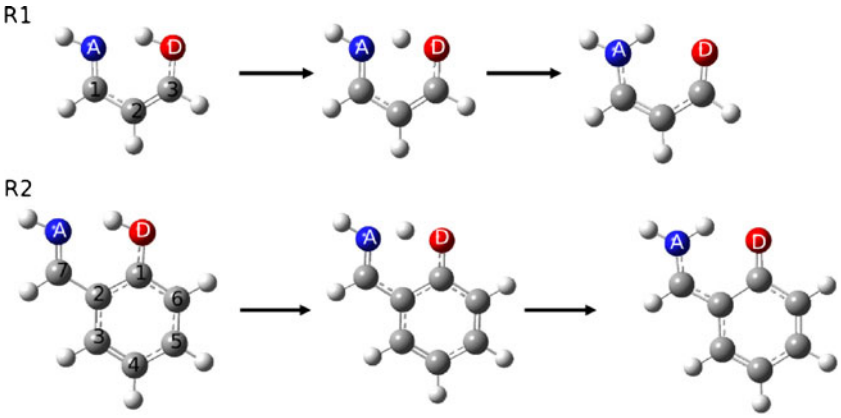

Fig. 1 Proton transfers (**PT**) on 3-hidroxy-2-propenimine (**R1**), and salicylaldimine (**R2**)

double well potential where the first well holds the reactant (**R**) while second holds the product (**P**), it can be obtained by differenciation the reaction force profile. This concept leads to the definition of different regions along the reaction coordinate [2, 13–15], in which different reaction mechanisms might be operating. To each of these regions there are associated specific amounts of work that can be calculated by integrating the force profile within the specific region, this allows the quantification of the energy cost of each step of the reaction. The electronic activity is analyzed in terms of the reaction electronic flux that identifies the regions along the reaction coordinate where electronic polarization and transfer are taking place. This quantity, obtained through the variation of electronic chemical potential (μ) with respect to the reaction coordinate gives; valuable insights about reaction mechanisms.

This paper is organized as follows: the next section is devoted to the definition of the concepts used in the analysis of the various systems. Then Computational details are presented, followed by Discussion of the results, and finally some Conclusions are drawn.

Theoretical background

Energy and force profiles

A chemical reaction occurs through the simultaneous change of different geometrical parameters onto a multidimensional space. This multidimensional motion is condensed into the intrinsic reaction coordinate IRC [16] (ξ), which measures the progress of the reaction going from reactant to products, and the energy profile along ξ being the result of the calculation following its minimum energy path. Numerical differentiation of $E(\xi)$ leads to the Hellman-Feynman reaction force [1, 14, 15, 17, 18]:

$$F(\xi) = -\frac{dE}{d\xi} \tag{1}$$

This is a global property of the reaction that contains information concerning the specific interactions that drive the reaction from reactants to products [1, 17]. Being the derivative of the energy profile, $F(\xi)$ may present several critical points, depending on the shape of the energy profile. These critical points define different regions along ξ in which different processes might be taking place. For a double well potential energy profile, the reaction force present two key points along ξ: the force minimum is located at ξ_1 and the force maximum at ξ_2, these points define regions that can be interpreted as involving preparation of reactant in the reactant region ($\xi_R \leq \xi \leq \xi_1$); transition to product in the transition state region ($\xi_1 < \xi < \xi_2$) and relaxation of the product species in the product region ($\xi_2 \leq \xi \leq \xi_P$). Three regions are therefore identified in a generic double-well potential energy profile the reactants, transition state and product regions [1, 14, 18].

Chemical potential and electronic flux

Within the conceptual framework of DFT, the chemical potential of a system of N particles with total energy E and external potential $v(\mathbf{r})$ is defined as [19]:

$$\mu = \left(\frac{\partial E}{\partial N}\right)_{v(r)} = -\chi, \tag{2}$$

In Eq. 2, χ is the electronegativity [20–25]. Owing to the discontinuity of the variable N, chemical potential is not possible to obtain by differenciation. It must be calculated using approximations, such as the use of finite difference approximation and Janak's theorem through the following expressions [26]

$$\mu \approx -\frac{1}{2}(\mathrm{I} + \mathrm{A}) \cong \frac{1}{2}(\varepsilon_{\mathrm{L}} + \varepsilon_{\mathrm{H}}), \tag{3}$$

where I is the first ionization potential, A is the electron affinity; ε_L and ε_H are the energies of the lowest unoccupied and highest occupied molecular orbitals, LUMO and HOMO, respectively. By evaluating μ along the reaction

coordinate it is possible to determine the profile $\mu(\xi)$ that shows the evolution of the chemical potential during the chemical reaction.

The underlying principle behind the electronic transfer is the relationship between the electronic flux and a charge density gradient, in this context, the reaction electronic flux (REF) associated to a chemical reaction is defined as [11, 12, 17]:

$$J(\xi) = -Q\frac{d\mu}{d\xi} \tag{4}$$

Where Q is analog to a transport coefficient [17], it can be estimated from the reaction energies and chemical potential. The profile of $J(\xi)$ is quite useful in the identification of regions along the reaction coordinate that are characterized by electronic reordering and transfer. In analogy to classic thermodynamics, the regions with $J(\xi)>0$ are associated to spontaneous rearrangement of the electronic density; whereas regions with $J(\xi)<0$ should be associated to nonspontaneous reordering of the electronic density.

In a recent paper, a flux decomposition in terms of polarization and transfer fluxes was proposed [27]:

$$J(\xi) = J_p(\xi) + J_t(\xi) \tag{5}$$

It was proposed that polarization flux can be calculated considering the reactive complex separated into fragments, for instance, a binary reaction A+B, where the fragments are treated separately using the counterpoise method [28]. It can be obtained from the sum of fragment A and B fluxes:

$$J_p(\xi) = J_A(\xi) + J_B(\xi) = -Q_A\left(\frac{d\mu_A}{d\xi}\right) - Q_B\left(\frac{d\mu_B}{d\xi}\right) \tag{6}$$

$$\text{and} \quad J_t(\xi) = J(\xi) - J_p(\xi) \tag{7}$$

Being μ_A and μ_B the chemical potentials of the perturbed isolated molecules A and B along the reaction path, thus polarization flux describes the deformation of the electronic cloud of fragment A in the presence of fragment B and viceversa. It has been previously demonstrated that this polarization effect can be noted markedly at the preparation or relaxation steps of reactions [27, 29]. $J_t(\xi)$ accounts for the electronic transfer among the fragments. With all this information along with a suitable bond order analysis, a chemical reaction can be described accurately along the reaction coordinate.

Computational details

The proton transfer in **R1** and **R2** has been characterized by means of theoretical calculations along the intrinsic reaction coordinate IRC, using the *Gaussian 03* [30] package. The minimum energy path followed by the protons transferred from donor to acceptor atoms lie at the molecular plane. The donor-acceptor pairs labelled {D,A} are shown in Fig. 1. The IRC calculations were performed at DFT/B3LYP/6-311+G** level; then using the optimized geometries obtained from the IRC procedure, molecular properties were determined through single point calculations at the same level. Mulliken population analysis was performed at B3LYP/6-311G** level, due to the poor performance of Mulliken analysis with diffuse functions. Frequency calculations of reactants, transition states and products were performed to confirm the nature of the critical points along the reaction path.

To obtain the REF, chemical potential was obtained using Eq. 3 and frontier molecular orbital energies ε_H and ε_L, J_p was calculated using the counterpoise method [28], where **R1** and **R2** were fragmented arbitrarily into two, considering a donor fragment and an acceptor fragment (See Fig. 2). In this way, chemical potential of both fragments was calculated along the reaction coordinate using the geometry obtained at the IRC procedure at DFT/B3LYP/6-311+G** methodology. Having $\mu_A(\xi)$ and $\mu_B(\xi)$ from the counterpoise routine, the polarization J_p and transfer J_t fluxes were calculated using Eqs. 6 and 7.

Results and discussion

Energy and force profiles

In Fig. 3 are shown the energy and reaction force profiles for **R1** and **R2**. As this figure shows, both processes have different thermochemistry, **R1** is exoenergetic with a low energy barrier (1.5 kcal/mol) which indicates an imino-enol reactant (**R**) that can be converted to a more stable amino-oxy system at room temperature. **R2** is endoenergetic with

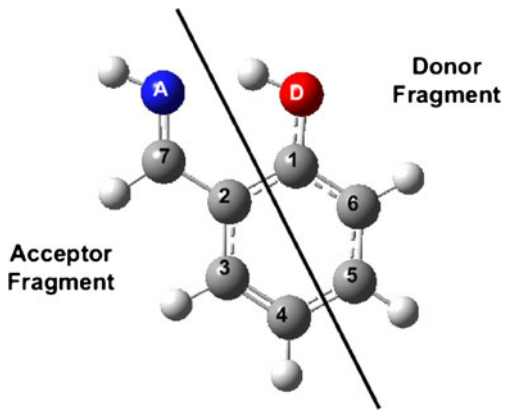

Fig. 2 Acceptor and donor fragments of the systems considered at counterpoise metod

a higher energy barrier (6 kcal/mol). At least from the energetic point of view both reactions bear as the opposite to each other. The aromatic cycle in salicylaldimine stabilizes the reactant with respect to the product and raises the energy barrier with respect to that observed in **R1**. In summary, while **R1** presents a favorable thermodynamic and kinetic control, **R2** is unfavorable both thermodinamically and kinetically [31].

The concept of reaction mechanism is related to the nuclear displacements and electronic reordering in going from **R** to **P**. To elucidate the mechanism, the reaction force was obtained form Eq. 1 and their profiles are also displayed in Fig. 3. As already mentioned, the critical points of F(ξ) define regions where the specific interactions driving the reaction might be of a different nature [11–13]. As Table 1 shows, the first step of the reaction requires an amount of work $W_1 = \int_{\xi_R}^{\xi 1} F(\xi)d\xi$, necessary to bring donor and acceptor atoms close to each other. This work is different in magnitude for **R1** and **R2**, probably caused by the aromaticity of the ring in the reactant structure of **R2** (**R@R2**), but amazingly it corresponds in both cases to 66% of the total energy barrier. The activation works W_1 represent in both reactions the same proportion of the activation energy, thus indicating a common feature even though the reaction are opposite from the thermodinamic and kinetic (opposite barriers) viewpoints [31].

The second step which is associated to electronic reorganization of the reaction, involves the total TS work, composed by an activation work $W_2 = -\int_{\xi 1}^{\xi_{TS}} F(\xi)d\xi$ and relaxation $W_3 = -\int_{\xi_{TS}}^{\xi 2} F(\xi)d\xi$. When analyzing the W_2 values for **R1** and **R2**, it can be distinguished that the aromaticity of **R2** also influences this parameter, having higher W_2 than **R1**. W_3 indicates that the formation of **P@R2** starts to be unfavorable, indicating reversibility at this last reaction, which is emphasized with $W_4 = -\int_{\xi_2}^{\xi_P} F(\xi)d\xi$; values reflects that the stability of the **P@R1** is higher than **P@R2**. In summary, the

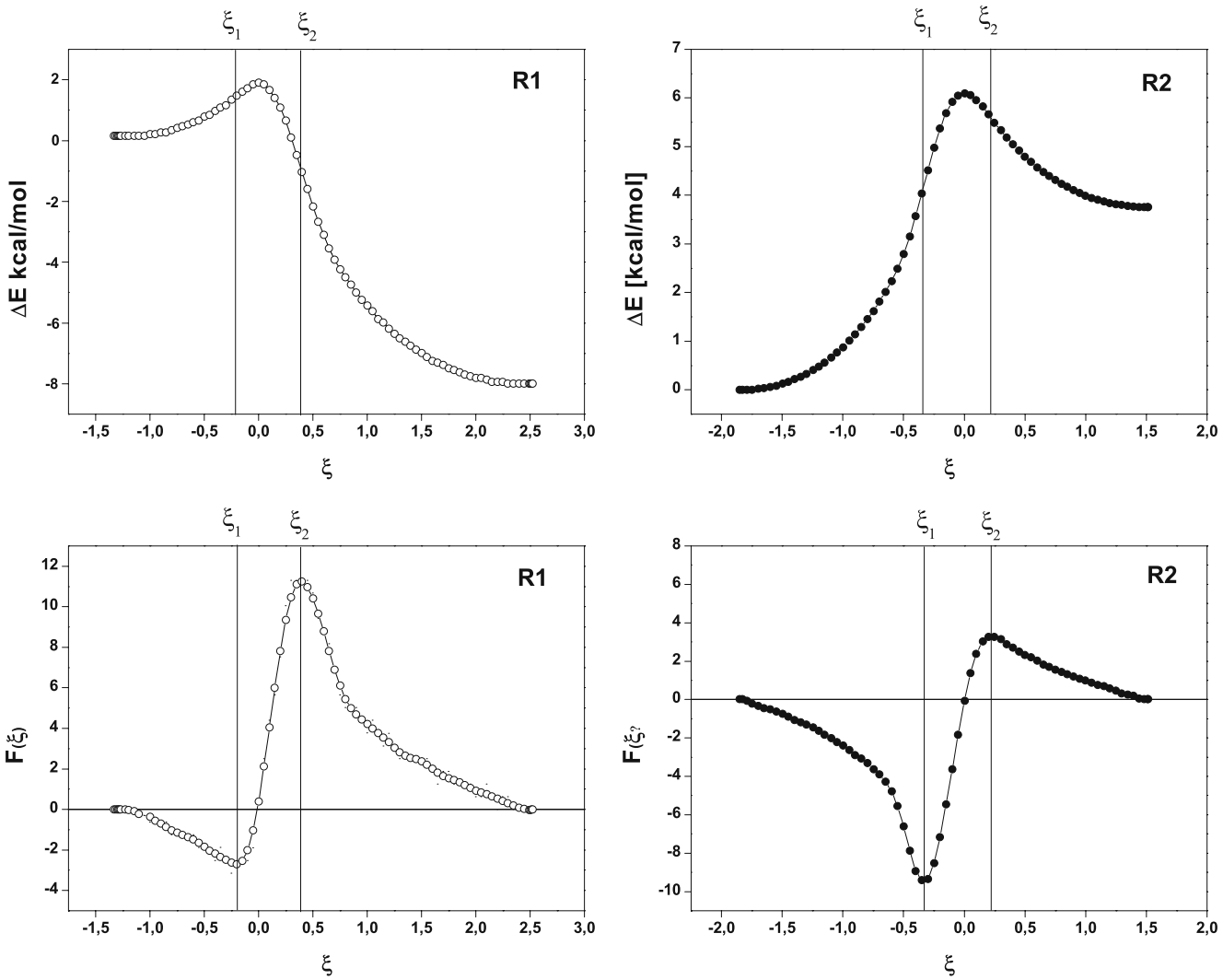

Fig. 3 Potential energy and force profiles for **R1** (open dots) and **R2** (filled dots)

Table 1 Works implicated at R1 and R2

System	W1	W2	W3	W4
R1	1.16	0.60	-2.95	-6.97
R2	4.04	2.06	-0.76	-1.57

presence of the neighbor ring increases the activation energy and its components by a factor of about 3.5. On the other hand, the ring destabilizes the product of reaction making **R2** endoenergetic by 3.80 kcal/mol. Thus, the role that the ring offers to the reaction is an augmentation of the PT barriers and works.

When comparing this 1–5 with 1–4 proton transfers from a previuos article [14] it can be noted that the spacing plays an interesting effect; while both ring 7 systems are rigid, the extra carbon atom of **R2** places the proton closer to the acceptor atom thus lowering the activation work. Unfortunatelly, there is no data published of $F(\xi)$ for aliphatic systems.

Structural rearrangement

When comparing the evolution along ξ of the backbone bond distances and angles that are displayed in Fig. 4, we note that the bond distances exhibit quite similar trends. Within the reactant region where C=N remains constant until entering the TS region, the C=N bond distances in **R1** and **R2** increase monotonically until reaching the product region. In contrast, the C-O distances start decreasing monotonically untill reaching the product region, where they remain constant. The C-O and C=N curves cross each other near ξ_{TS} and this movement allows the following proton transfer. The C-O decrease is the loss of double-bond character

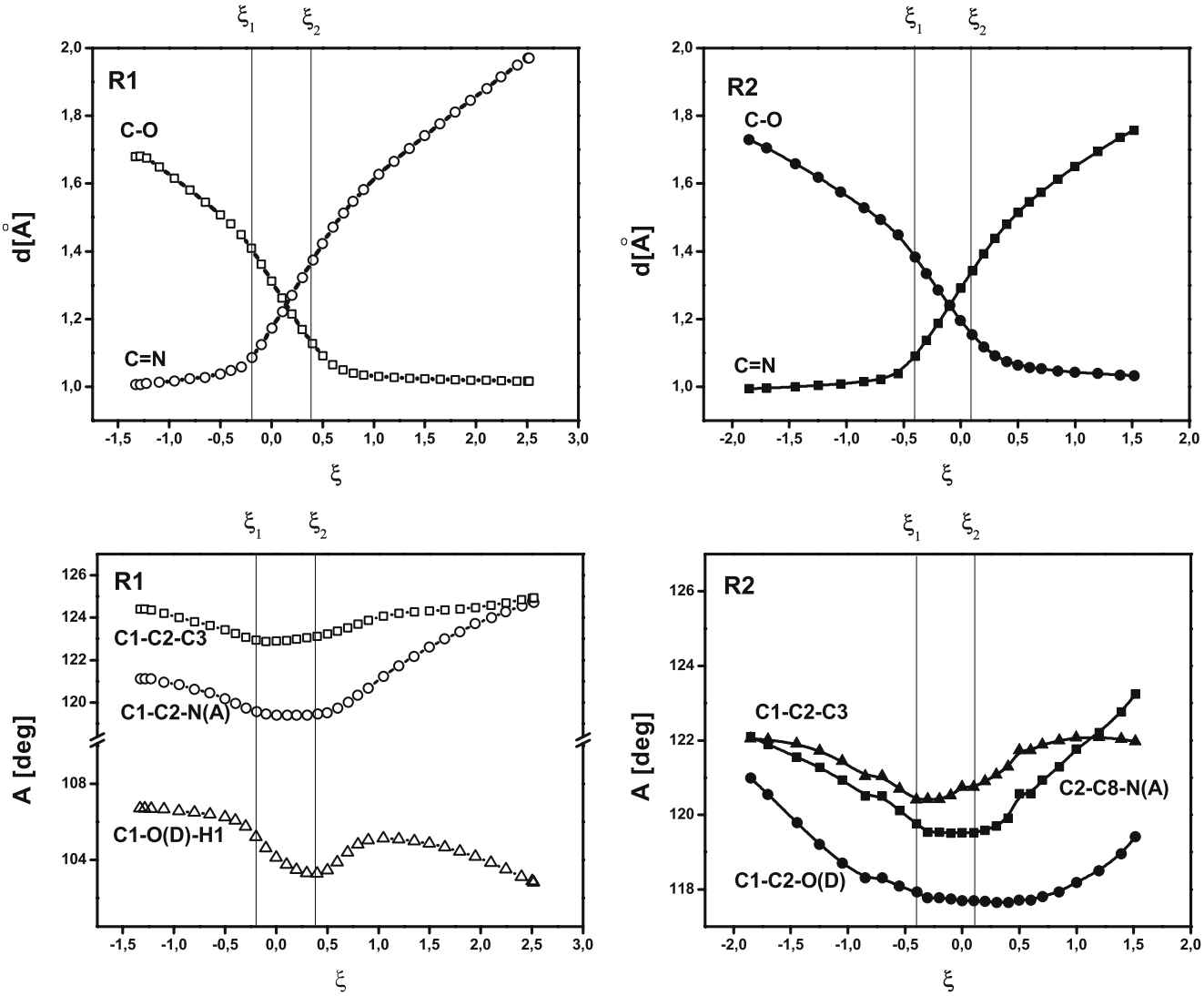

Fig. 4 Angle bendings in degrees, and bond stretchings (Å) for **R1** (open dots) and **R2** (filled dots)

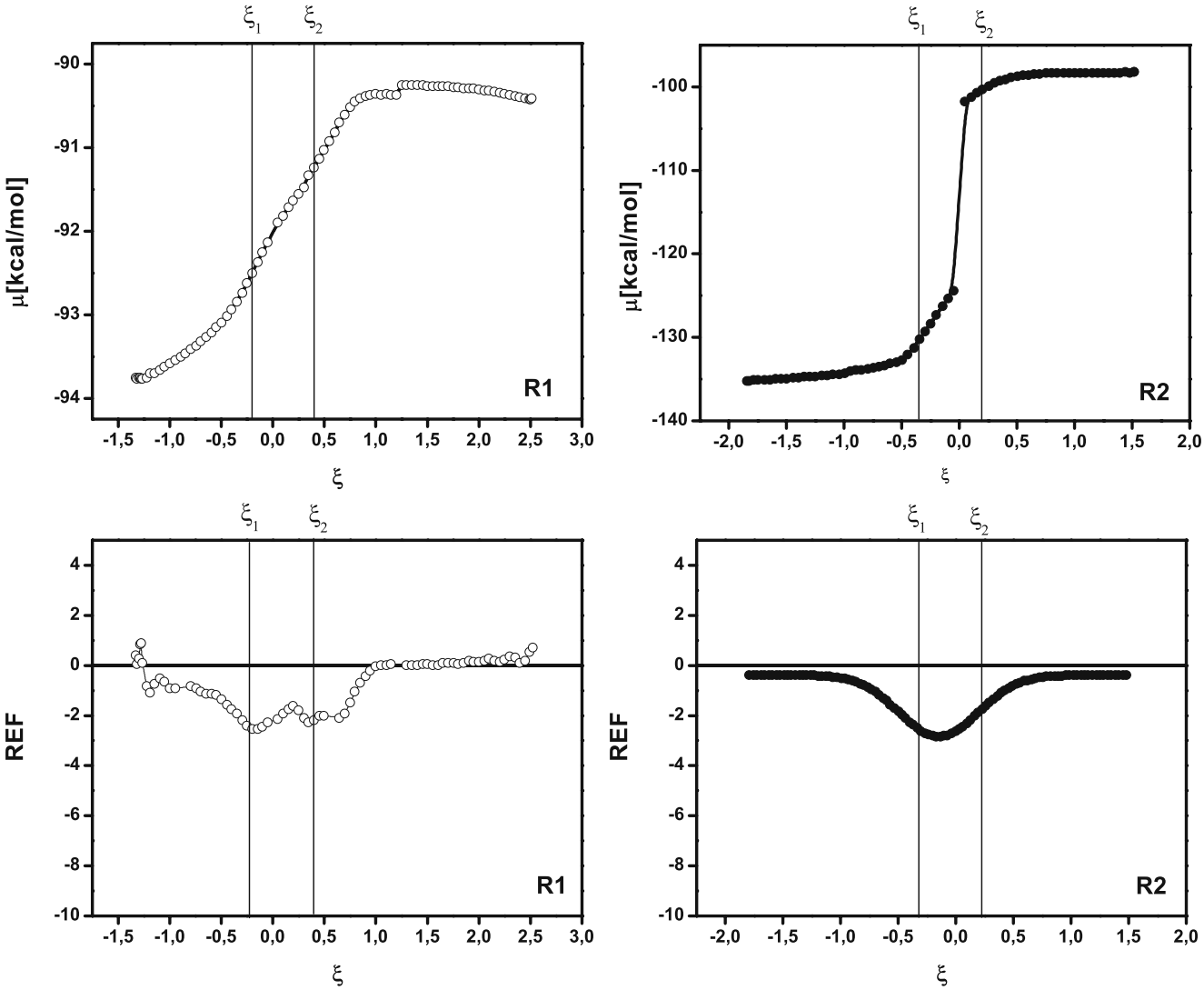

Fig. 5 μ in kcal/mol and reaction electronic flux (**REF**, J(ξ)) for **R1** (open dots) and **R2** (filled dots)

whereas the C=N increase should be attributed to the gain of double-bond character.

When analyzing the evolution of the angles involved at the PT in **R1** and **R2**, it becomes evident that these are the reactive modes that activate the hydrogen transfer. In particular, the backbone angles **C3-O(D)-H@R1; C3-C2-N(A)@R1**, and **C1-C2-C3@R2,C2-C7-N(A)@R2,C2-C1-O(D)@R2** change coupledly in order to allow the PT. In the reactant regions, these angles decrease allowing the donor and acceptor atoms to get closer to each other thus activating the transfer; the energetic cost associated is $\mathbf{W}_1$=1,16 kcal/mol in **R1** and $\mathbf{W}_1$=4,04 kcal/mol in **R2**. Within the **TS** region, the bond angles change slightly to allow the hydrogenic motion, suggesting that some of the nature of the overall **TS** work on **R1** might also be associated to a structural backbone rearrangement. At the product region the structural relaxation causes them to increase to reach the equilibrium value of the product molecule, this increase is more sharply in **R2** than **R1**. Note that the change of these three angles in **R2** is less than in **R1** due to the rigidity of the former system.

Chemical potential and reaction flux: Electronic transfer

In Fig. 5 are depicted the electronic chemical potentials (μ) along ξ, for **R1** and **R2**, as chemical potential indicates the electron flux from sites of high μ to sites of lower μ; these figures indicate that the nature of the electronic reordering is different for both systems; along the reaction coordinate is much larger in **R2** than in **R1** thus indicating a large electronic activity taking place in **R2**. In μ increases monotonically fom **R@R1** to ξ_2 where it reaches a quite constant value fading out to **P@R1**, this is due to the modification of the conjugation in the imino-enol reactant

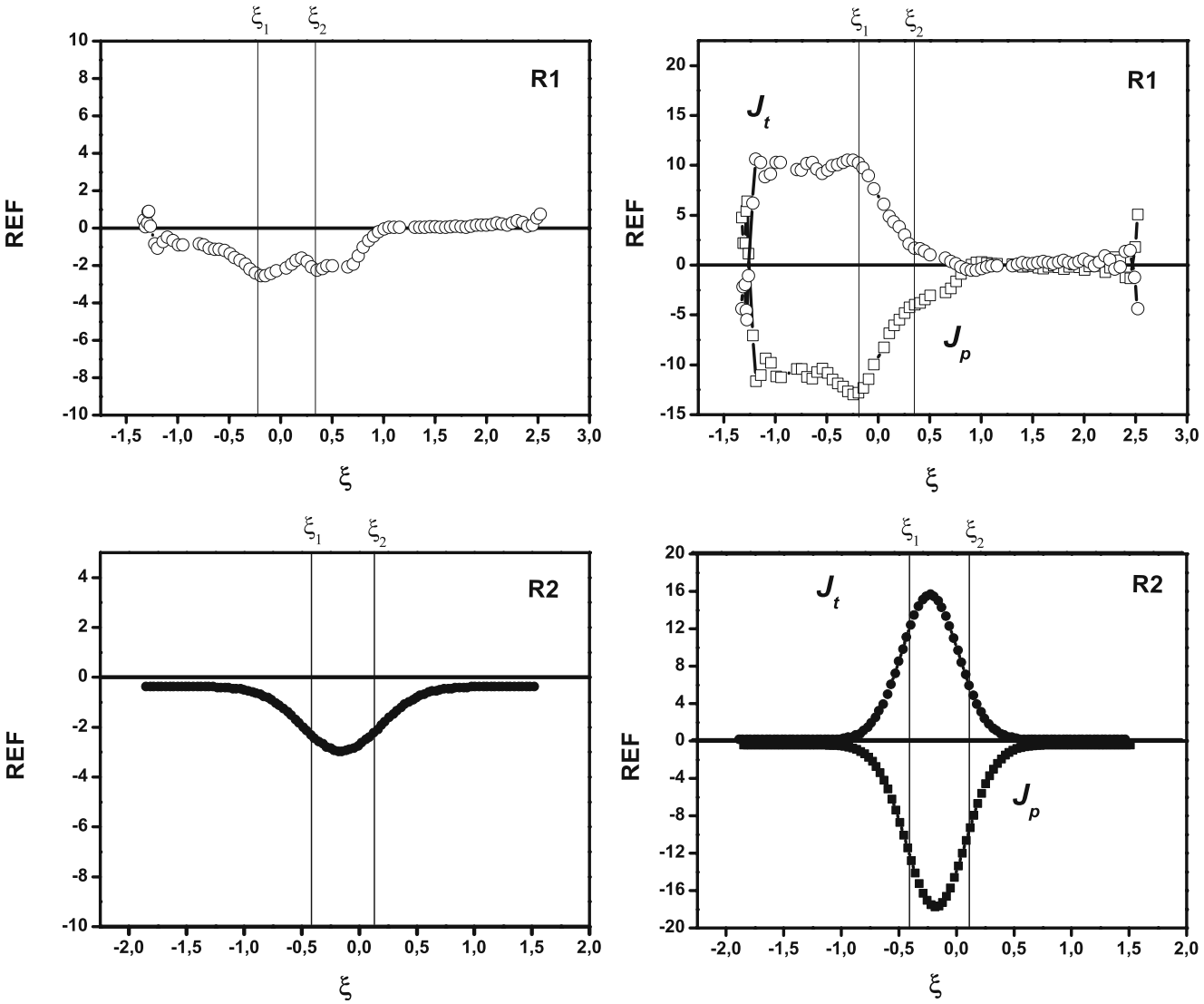

Fig. 6 Total electronic flux (**REF**, J(ξ)), transfer (J_t) and polarization flux (J_P) for **R1** (open) and **R2** (filled)

which is changed to an energetically more stable amino-oxy system. On the contrary, in **R2** μ starts from quite constant values at R due to the aromaticity of the system, then it highly increases at **TS@R2** zone and reaches almost a plateau at the relaxation zone which is less stable than the reactant due to the loss of aromaticity by the transformation to a *quinoidal* structure.

The electronic reordering during both PT is better appreciated when analyzing the reaction electronic flux (REF). Figure 5 shows that in **R1** and **R2** the REF presents a similar behavior in both cases a negative flux features around the transition state [11], thus indicating that the most important electronic reorganization occurs at the **TS** region of the transfer where bonds are broken and rearrange in order to allow the proton transfer.

In **R1** the REF profile presents two minima suggesting that the electronic reordering is stepwise whereas in **R2** it seems to be more synchronic due to the help that the ring offers to the electronic rearrangement. **R@R1** shows a monotonic decrease on J(ξ), while **R@R2** shows a plateau emphasizing the stability that the ring offers to the system, due to conjugation. At **TS@R1** the flux increases slightly to a tiny minimum that agrees with the bending at donor atoms angle (**C3-O(D)-H**) that helps the transfer at this zone. Moreover, from ξ_2 to **P@R2**, the electronic transfer decreases reaching zero values at the end of the transfer, indicating that even though the electronic transfer is high, it stops at ξ_2. The zero flux regime is present at **R@R2** and **P@R2**. In **R2** the electronic reordering is more localized at **TS** zone, as already observed on other proton transfers [11, 27, 32]. This constant flux might also be associated to resonance/aromatic behavior of the molecule.

As electronic flux indicated the steps that the electronic reordering follows at **R1** and **R2**; the electronic flux

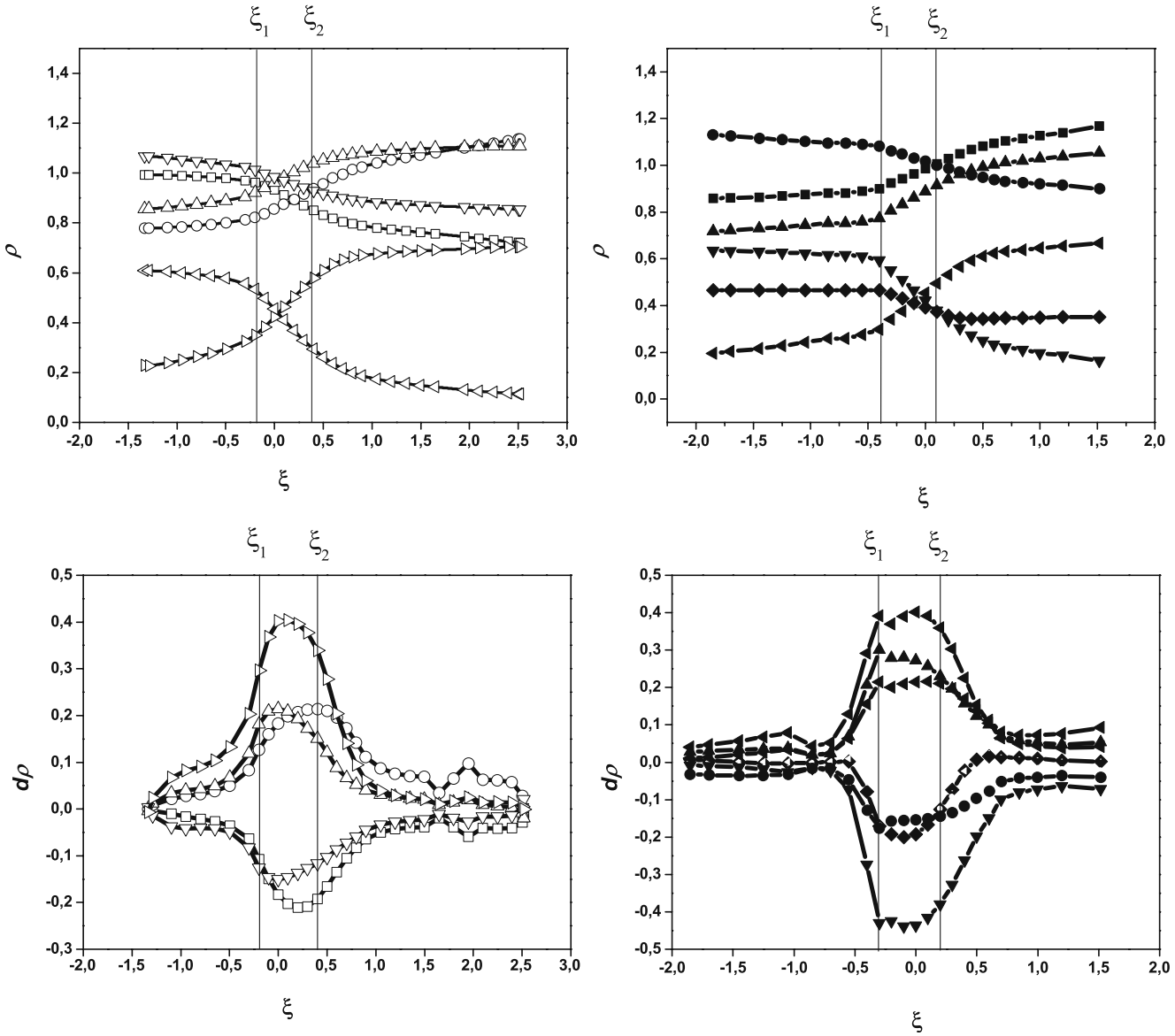

Fig. 7 Bond populations, in a. u (a) and Bond order derivatives (b) for R1 (open square, ρC1-C2; open circle, ρC1-DO; open triangle, ρC2-C4; open left triangle, ρH6-DO; open right triangle, ρN5-H6; filled down triangle, ρC4-N5) and R2 (filled circles, ρC7-AN; filled squares, ρC1-DO; filled triangle, ρC2-C7; filled down triangle _DO-H; filled rhombus ρC1-C2; filled left triangle, AN-H)

decomposition displayed at Fig. 6 will indicate the nature and the mechanism of the electronic reorganization at each reaction. At **R1** polarization and transfer fluxes indicate that at regions from **R@R1** to **TS@R1** the reaction electronic flux is mainly due to contributions of polarization and transfer, although at the sum of both contributions polarization dominates indicating that the activation of **R1** is due to a deformation of the electronic cloud. From ξ_2 the electronic transfer stops and only polarization remains entering the product region. Having all the previously discussed data at hand, this reaction is activated at **R@R1** by the bending of the molecule which reorganizes the electronic distribution through polarization that instanta-

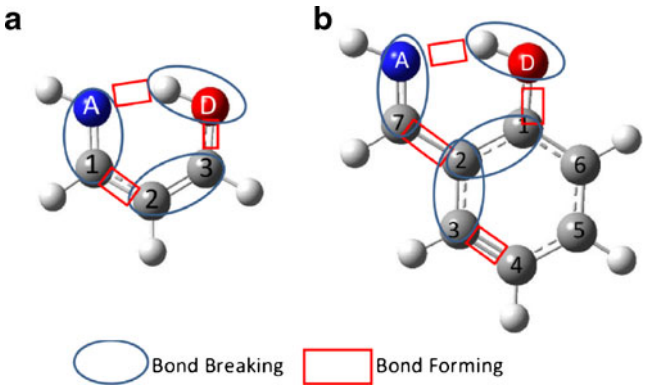

Fig. 8 Bond breaking and forming scheme for (a, **R1**) and (b, **R2**)

neously induces electronic transfer to allow the proton transfer.

Figure 6 compares both polarization and transfer contributions to the total flux at **R2**; the overall electronic at the reactant zone is constant and slightly negative; indicating some polarization composition, this implies that this reaction, has an electronic reordering that only starts at **TS@R2** mainly composed by polarization as this figure indicates. Then at **P@R2** there is some transfer flux that lowers the constant values of the overall flux, indicating electronic 9 transfer between the fragments as a signature of electronic delocalization. In this reactopm; at the light of the results already discussed in Structural rearrangement and Chemical potential and reaction flux: Electronic transfer; the ring seemps to split the geometry and electronic rearrangements at W_1 which characterize the aliphatic system.

Bond order analysis

In Fig. 7 are depicted the most representative bond populations for **R1** and **R2**. It can be observed that the highest intensity of bond populations reordering takes place at the TS region.

When analyzing the bond population derivatives depicted in Fig. 6 to understand the rates of dissociation and formation of bonds, it can be noted that at **R1** bond breaking and forming at **R@R1** start changing and they are balanced in quantity. However, from ξ_1 A-H forming (left triangles) is leading at this stage of the reaction. Then reordering at ξ_2 starts decreasing at **P@R1** where the reaction stops.

At **R2**, the bond breaking and forming is quite constant at **R@R2**, near ξ_1 the reordering starts only at the **TS@R2** the bonds start to reorder in order to achieve the PT, only ρ_{C3-C4}, ρ_{C1-OD} remain constant at this zone. At **P@R2** all the populations end the reordering in order to form products with practically no change in the bond order. It is interesting to note that in both reactions the bond populations are forming and dissociating following a synchronized pattern, indicating that in both cases the double bond conjugation plays an important role helping electron reordering. While **A-H** starts forming, it triggers electron delocalization and a synchronized bond breaking/forming, specially at the **TS**. See Fig. 8.

Concluding remarks

In this work we have analyzed and characterized the mechanism of 1–5 proton transfers was completely characterized by the analysis of energy, reaction force profile, chemical potential and REF within the frame of the density functional theory, obtaining the reaction mechanism of aliphatic or ring-assisted 1–5 proton transfers. It was found that both reactions behave with opposite thermochemistry and kinetics. The ring influences **R2** process making it reversible due to the low reverse barrier.

Also, when analyzing the REF, it was also found that the nature of electronic transfer changes with the vicinity of an aromatic ring, at **R1** the electronic flux indicates that the reordering is stepwise and coupled with structural rearrangement.

At **R2** this is synchronic due to the help that the ring offers 10 to the PT, also the vicinity of the ring originates a plateau at **P@R2** which is associated to the conjugation of the final product. REF for both reactions is mostly associated to polarization effects indicating that electronic delocalization is the phenomena that helps electronic reordering specially at the **TS** zone. This observation is reinforced with the use of ρ derivatives at the bond order analysis, they indicate that double bond conjugation played an important role helping the electronic reordering.

It was found comparing **R2** with previous 1–4 proton transfer works [14] that although both systems are rigid, the carbon atom spacer of **R2**, lowers the barrier, thus W_1 and W_2 due to the proximity of the proton to the acceptor atom.

Acknowledgements This work was supported by FONDECYT under grants #11080002 and #1090460. Thanks to Dr. Alejandro Toro-Labbe for helpfull comments.

References

1. Jaque P, Toro-Labbé A (2000) J Phys Chem A 104:995–1003
2. Herrera B, Toro-Labbé A (2004) J Phys Chem A 108:1830–1836
3. Catalán J, Toribio F, Acunã AU (1982) J Phys Chem 86:303–306
4. Acunã AU, Toribio F, Amat-Guerri F, Catalán J (1985) J Photochem 30:339–352
5. Toribio F, Catalán J, Amat-Guerri F, Acunã AU (1983) J Phys Chem 87:817–822
6. Heimbrook LA, Kenny JE, Kohler BE, Scott GW (1983) J Phys Chem 87:280–289
7. Kuper JW, Perry D (1984) J Chem Phys 80:4640–4646
8. Rodríguez-Santiago L, Sodupe M, Bertrán J (1999) J Am Chem Soc 121:8882–8890
9. Orton E, Pimentel GC (1990) J Phys Chem 94:7936–7943
10. Felker PM, Lambert WR, Zewail AH (1982) J Chem Phys 77:1603–1606
11. Herrera B, Toro-Labbé A (2007) Phys Chem A 111:5921–5926
12. Flores P, Gutiérrez-Oliva S, Herrera B, Toro-Labbé A (2007) AIP Conf Proc 963:345–349
13. Gutiérrez-Oliva S, Herrera B, Toro-Labbé A, Chermette H (2005) J Phys Chem A 109:1748–1751
14. Herrera B, Toro-Labbé A (2004) J Chem Phys 121:7096–7102
15. Toro-Labbé A, Gutiérrez-Oliva S, Concha MC, Murray J, Politzer P (2004) J Chem Phys 121:4570–4576
16. Fukui K (1981) Acc Chem Res 14:363–368
17. Toro-Labbé A (1999) J Phys Chem A 103:4398–4403
18. Martínez J, Toro-Labbé A (2004) Chem Phys Lett 392:132–139
19. Parr RG, Yang W (1989) Density functional theory of atoms and molecules. Oxford University Press, New York, USA

20. Sen KD, Jorgensen CK (1987) Electronegativity: structure and bonding, vol 66. Springer Verlag, Berlin, Germany
21. Pauling L (1960) The nature of chemical bond. Cornell University Press, New York, USA
22. Pearson RG (1990) Coord Chem Rev 100:403–425
23. Pearson RG (1973) Hard and soft acid and bases. Dowden, Hutchinson and Ross, Stroudsberg, USA
24. Ayers PW, Parr R (2000) J Am Chem Soc 122:2010–2018
25. Pearson RG (1985) J Am Chem Soc 107:6801–6806
26. Geerlings P, Proft FD, Langenaeker W (2003) Chem Rev 103:1793–1874
27. Echegaray E, Toro-Labbé A (2008) J Phys Chem A 112:11801
28. Boys SF, Bernardi F (1970) Mol Phys 19:553–566
29. Vogt-Geisse S, Toro-Labbé A (2009) J Chem Phys 130:244308–2443081
30. Frisch MJ, Trucks GW, Schlegel HB, Scuseria GE, Robb MA, Cheeseman JR, Montgomery JA, Vreven T, Kudin KN, Burant JC, Millam JM, Iyengar SS, Tomasi J, Barone V, Mennucci B, Cossi M, Scalmani G, Rega N, Petersson GA, Nakatsuji H, Hada M, Ehara M, Toyota K, Fukuda R, Hasegaw J, Ishida M, Nakajima T, Honda Y, Kitao O, Nakai H, Klene M, Li X, Knox JE, Hratchian HP, Cross JB, Adamo C, Jaramillo J, Gomperts R, Stratmann RE, Yazyev O, Austin AJ, Cammi R, Pomelli C, Ochterski JW, Ayala PY, Morokuma K, Voth GA, Salvador P, Dannenberg JJ, Zakrzewski VG, Dapprich S, Daniels AD, Strain MC, Farkas O, Malick DK, Rabuck AD, Raghavachari K, Foresman JB, Ortiz JV, Cui Q, Baboul AG, Clifford S, Cioslowski J, Stefanov BB, Liu G, Liashenko A, Piskorz P, Komaromi I, Martin RL, Fox DJ, Keith T, Al-Laham MA, Peng CY, Nanayakkara A, Challacombe M, Gill PMW, Johnson B, Chen W, Wong MW, Gonzalez C, Pople JA (2003) Gaussian Inc, Pittsburgh, PA
31. Fessenden RJ, Fessenden JS (1982) Organic chemistry. PBS, Boston, USA
32. Parra RD, Dukarevich I (2005) J Chem Phys 122:124316